J|A|C|S
COMMUNICATIONS

Published on Web 04/10/2004

Spectroscopic and Quantum Chemical Characterization of the Electronic Structure and Bonding in a Non-Heme Fe^{IV}═O Complex

Andrea Decker,† Jan-Uwe Rohde,‡ Lawrence Que, Jr.,*,‡ and Edward I. Solomon*,†

Department of Chemistry, Stanford University, Stanford, California 94305, and Department of Chemistry and Center for Metals in Biocatalysis, University of Minnesota, Minneapolis, Minnesota 55455

Received January 12, 2004; E-mail: Edward.Solomon@stanford.edu; que@chem.umn.edu

The catalytic pathways of many mononuclear non-heme iron enzymes are proposed to involve a high-valent iron-oxo intermediate as the active oxidizing species.[1,2] Such an intermediate is an integral part in many heme enzymatic cycles.[3,4] Thus far, only for one non-heme iron enzyme (TauD) has an iron(IV) intermediate been trapped.[5] Several iron(IV)-oxo model complexes with non-heme ligand sets have now been synthesized and characterized,[6−9] all with a six-coordinate axially distorted center and an $S = 1$ ground state. Using variable temperature magnetic circular dichroism (VT MCD) spectroscopy and experimentally calibrated density functional calculations, we are able to present the first detailed electronic structure description of a non-heme Fe^{IV}═O complex. These studies define the nature of the Fe^{IV}═O bond and present the basis for understanding high-valent intermediates in non-heme iron enzymes.

The −40 °C acetonitrile solution absorption spectrum of $[Fe(O)(TMC)(NCCH_3)]^{2+}$ (Figure 1A)[10] shows a broad asymmetric feature at ∼12 000 cm^{-1} (ϵ = 400 M^{-1} cm^{-1}), a weaker signal around 18 000 cm^{-1} ($\epsilon \approx$ 40 M^{-1} cm^{-1}), and a steep intensity increase starting at ∼24 000 cm^{-1}. The mull MCD spectra of the same species were taken at 7T and a series of temperatures (Figure 1B). The 2K (blue) MCD spectrum contains band I in the 9000−12 000 cm^{-1} region, a weaker band IV at ∼17 000 cm^{-1}, and an intense band V at ∼25 000 cm^{-1}. Superimposed on band I is a progression starting at ∼8100 cm^{-1}. With increasing temperature, the intensities of bands I and V decrease, while two features increase: a negative signal at ∼10 500 cm^{-1} (band II, see Supporting Information) and a positive one at ∼13 000 cm^{-1} (band III). Their intensities reach a maximum at ∼20 K and then decrease with further increase in temperature. All MCD features show linear dependence with magnetic field strength.

These different temperature-dependent behaviors in the MCD reflect different polarizations of electronic transitions. MCD intensity is proportional to $g_i M_j M_k$, where g_i is the Zeeman effect in i direction, M_j, M_k are electric dipole transition moments in j, k directions, and i, j, k are cyclic permutations of x, y, z. This complex was defined by Mössbauer studies[7] as an axial distorted octahedron with an $S = 1$ ground state and a positive zero-field splitting, $D > 0$, between the nondegenerate $M_S = 0$ and the doubly degenerate $M_S = \pm 1$ sublevels (Figure 1C; D(Mössbauer) = +29 cm^{-1};[7] D(VT MCD) = +26 cm^{-1})). For xy-polarized transitions, MCD intensity is present only with the magnetic field H in the z-direction (Figure 1C, left). In this field orientation, the $M_S = 0$ level does not mix with other M_S sublevels, and thus there is no MCD signal at low temperatures. Increasing temperature populates the $M_S = \pm 1$ levels, which are MCD active, and xy-polarized transitions gain MCD intensity. For z-polarized transitions, the magnetic field must be in the xy-plane for MCD intensity (Figure 1C, right). In this orientation, the $M_S = 0$ level mixes with one component of $M_S = \pm 1$ and

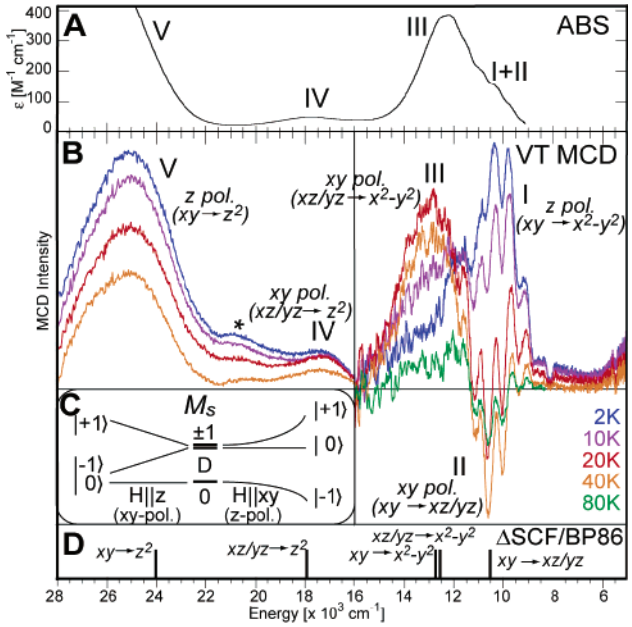

Figure 1. Electronic absorption (A) and VT MCD spectra (B) with selection rules (C) and calculated transition energies (D) of $[Fe(O)(TMC)(NCCH_3)]^{2+}$.

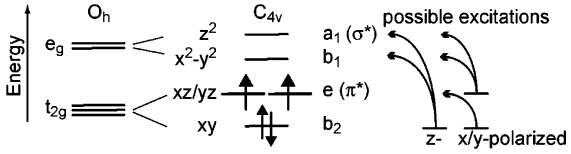

Figure 2. Ligand field splitting diagram and allowed d−d transitions.

induces MCD intensity into the lowest level at low temperatures. Increasing temperature decreases the population of this level, and the MCD intensity decreases. Thus, starting at low temperatures, xy-polarized transition intensity increases with temperature, while z-polarized transition intensity decreases.

The temperature behavior of the MCD features allows us to assign polarizations to bands in a randomly oriented sample: Bands I and V are z-polarized transitions, while bands II and III are xy-polarized transitions. Since band IV overlaps with bands III and V, its temperature behavior and thus polarization are difficult to distinguish.

According to group theory, a d^4 $S = 1$ system with C_{4v} symmetry has a $^3A_2$ ground state with five spin allowed, electric dipole allowed d−d ligand field transitions (Figure 2). Specific assignments can be made based on the polarization of the bands deduced from their MCD temperature behavior, vibronic structure, and their relative intensities in the electronic absorption spectrum.

Band I is assigned to the z-polarized $d_{xy} \rightarrow d_{x^2-y^2}$ transition reflecting the equatorial ligand field strength. Importantly, this transition is observed at a much lower energy than expected from

† Stanford University.
‡ University of Minnesota.

10.1021/ja0498033 CCC: $27.50

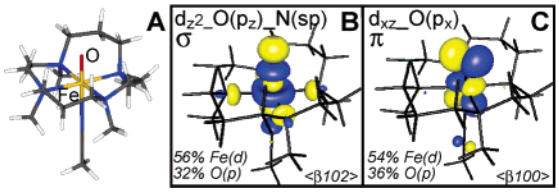

Figure 3. Optimized geometry of $[Fe(O)(TMC)(NCCH_3)]^{2+}$ and contour plots of the orbitals involved in iron-oxo σ- and π-bonding.

a one-electron orbital picture (Figure 2). The excited state is stabilized significantly by the reduction of electron−electron repulsion due to the excitation of an electron out of a doubly occupied, pure *d*-orbital, localized on the metal (d_{xy}) into an unoccupied orbital, partly delocalized onto the equatorial ligands ($d_{x^2-y^2}$). Thus, electron−electron repulsion must be taken into account for the correlation between many-electron excited-state transition energies and one-electron orbital diagrams.

Band II (negative in MCD and weak in Abs) and band III (positive in MCD and intense in Abs) are both *xy*-polarized. Band II is assigned to the $d_{xy} \rightarrow d_{xz/yz}$ transition. The $d_{xy} \rightarrow d_{xz/yz}$ transition reflects the oxo-iron π-bond strength, i.e., two 1/2 π-bonds (Figure 2). The transition energy of ~10 500 cm^{-1} is underestimated for the 1 e^- orbital splitting, since the electron−electron repulsion is reduced by delocalization of the $d_{xz/yz}$ orbital. A negative progression appears to be associated with this transition. Excitation of an electron from the nonbonding d_{xy} orbital to the Fe−O π-antibonding $d_{xz/yz}$ orbitals weakens the Fe−O bond and would lead to a vibrational progression in the Fe−O stretching mode.

Band III is assigned to the $d_{xz/yz} \rightarrow d_{x^2-y^2}$ transition. This transition is intense in the absorption spectrum (Figure 1A), because of mixing with a low-lying very intense ligand-to-metal charge-transfer (LMCT) excited state.

Band IV is assigned to the *xy*-polarized $d_{xz/yz} \rightarrow d_{z^2}$ transition. The energy difference between band III and IV (4500 cm^{-1}) corresponds to the splitting of the e_g set caused by the σ^* interaction of the oxo ligand. The absorption intensity of band V is too low at 25 000 cm^{-1} for the lowest energy LMCT transition, the very intense $O\pi(p_x/p_y) \rightarrow Fe\pi(d_{xz/yz})$. Thus, band V is assigned to the highest energy ligand field transition, $d_{xy} \rightarrow d_{z^2}$, reflecting the strength of the oxo-iron σ-bond.

The MCD spectroscopy allows us to quantify the bonding and to distinguish between π- and σ-bonding contributions of the iron-oxo bond. It shows a very covalent, strong π-bond and a σ-bond considerably stronger than typical Fe−N σ-interactions as reflected by the splitting of the e_g set.

Density functional calculations have been performed using the ADF program.[11] The fully geometry-optimized structure of the $[Fe(O)(TMC)(NCCH_3)]^{2+}$ complex (Figure 3A, coordinates in Supporting Information) is in good agreement with the X-ray structure.[7] The calculated transition energies for the five spin allowed, electric dipole allowed transitions correspond well to the spectroscopic data (Figure 1D). We can thus use the calculations to gain further insight into the bonding of this and related non-heme ferryl systems.

The calculated energy splitting of the d_{xy} and $d_{xz/yz}$ orbitals (11 770 cm^{-1}) and the e_g set (5000 cm^{-1}), in addition to the large mixing of Fe(*d*) and O(*p*) orbitals (Figure 3B,C) support the notion of very strong, covalent iron-oxo π- and σ-bonds. The high covalency of the Fe−O π-bond is the origin of unpaired electron density on the O-atom (SI Table 2); a diradical $Fe^{III}{}_{LS}-O^-$ description[9] is not appropriate.

Using these experimentally calibrated DFT calculations, we can gain insight into the electronic structure, bonding, and spectroscopy of Fe^{IV}=O $S = 2$ species, key intermediates for many non-heme iron enzymes. The $S = 2$ state, in which the d_{xy}, d_{xz}, d_{yz}, and $d_{x^2-y^2}$ orbitals (in Figure 2) are singly occupied, is higher in energy by 13 kcal/mol. This value might be overestimated since pure DFT methods tend to favor low-spin states. The energy difference between the $S = 1$ and $S = 2$ states can be conceptually divided into three steps: (1) The excitation of an electron from the doubly occupied d_{xz} orbital into the $d_{x^2-y^2}$ orbital, which corresponds to the $d_{xy} \rightarrow d_{x^2-y^2}$ transition, band I at ~10 500 cm^{-1} (calculated at 12 500 cm^{-1}, 36 kcal/mol). (2) A spin-flip, giving an $S = 2$, which lowers the electron−electron repulsion and the energy by 18 kcal/mol. (3) The geometric relaxation from the $S = 1$ to the $S = 2$ equilibrium geometry, which is relatively small and further stabilizes the complex by 5 kcal/mol. Between the competing effects of ligand field splitting and electron−electron repulsion, the equatorial ligand field strength of this TMC ligand dominates and determines the ground state. Importantly, the iron-oxo bonding is the same in both the $S = 1$ and $S = 2$ species, since the d_{xy} and $d_{x^2-y^2}$ orbitals are perpendicular to the Fe−O bond and do not interact with the oxo ligand.[12] The calculated bond distances, vibrational frequencies, and orbital coefficients are comparable.

Combining spectroscopy with density functional calculations on the $S = 1$ complex, we can anticipate the general spectroscopic features of an Fe^{IV}=O $S = 2$ species: In a d^4 complex with C_{4v} symmetry there would be only one spin allowed/electric dipole allowed, *xy*-polarized d−d transition ($d_{xz/yz} \rightarrow d_{z^2}$) exhibiting an intense MCD band at a calculated transition energy of ~15 000 cm^{-1} for the TMC ligand set. Thus, while the spectroscopy of an Fe^{IV}=O $S = 2$ species should look very different from that of the $S = 1$ species presented and analyzed here, the nature of the iron-oxo bond and its activation should be very similar.

Through a combination of spectroscopy and quantum chemical calculations we have quantitatively defined the iron-oxo bond in a high valent mononuclear Fe^{IV}=O species and related it to possible enzyme intermediates.

Acknowledgment. This work was supported by NIH GM-40392 (E.I.S.), NIH GM-33162 (L.Q.), and a DFG postdoctoral fellowship (J.-U.R.). We thank the reviewers for thoughtful comments.

Supporting Information Available: Sample preparation, UV−vis and MCD spectroscopy, computational details, coordinates of optimized geometries, and key computational results (PDF). This material is available free of charge via the Internet at http://pubs.acs.org.

References

(1) Solomon, E. I.; Brunold, T. C.; Davis, M. I.; Kemsley, J. N.; Lee, S. K.; Lehnert, N.; Neese, F.; Skulan, A. J.; Yang, Y. S.; Zhou, J. *Chem. Rev.* **2000**, *100*, 235−349.
(2) Costas, M.; Mehn, M. P.; Jensen, M. P.; Que, L., Jr. *Chem. Rev.* **2004**, *104*, 939−986.
(3) Sono, M.; Roach, M. P.; Coulter, E. D.; Dawson, J. H. *Chem. Rev.* **1996**, *96*, 2841−2887.
(4) Ferguson-Miller, S.; Babcock, G. T. *Chem. Rev.* **1996**, *96*, 2889−2907.
(5) Price, J. C.; Barr, E. W.; Tirupati, B.; Bollinger, J. M.; Krebs, C. *Biochemistry* **2003**, *42*, 7497−7508.
(6) Grapperhaus, C. A.; Mienert, B.; Bill, E.; Weyhermuller, T.; Wieghardt, K. *Inorg. Chem.* **2000**, *39*, 5306−5317.
(7) Rohde, J.-U.; In, J.-H.; Lim, M. H.; Brennessel, W. W.; Bukowski, M. R.; Stubna, A.; Münck, E.; Nam, W.; Que, L., Jr. *Science* **2003**, *299*, 1037−1039.
(8) Lim, M. H.; Rohde, J. U.; Stubna, A.; Bukowski, M. R.; Costas, M.; Ho, R. Y. N.; Münck, E.; Nam, W.; Que, L., Jr. *Proc. Natl. Acad. Sci. U.S.A.* **2003**, *100*, 3665−3670.
(9) Balland, V.; Charlot, M.-F.; Banse, F.; Girerd, J.-J.; Mattioli, T. A.; Bill, E.; Bartoli, J.-F.; Battioni, P.; Mansuy, D. *Eur. J. Inorg. Chem.* **2004**, *2*, 301−308.
(10) For sample preparation, UV−vis, and MCD spectroscopy, see the Supporting Information.
(11) For computational details, see the Supporting Information.
(12) Lehnert, N.; Ho, R. Y. N.; Que, L., Jr.; Solomon, E. I. *J. Am. Chem. Soc.* **2001**, *123*, 8271−8290.

JA0498033